LASER INTERFEROMETER GRAVITATIONAL WAVE OBSERVATORY
- LIGO -
CALIFORNIA INSTITUTE OF TECHNOLOGY
MASSACHUSETTS INSTITUTE OF TECHNOLOGY

Technical Note	**LIGO-T1500218–v1**	2015/09/25

Prototyping a tilt-free seismometer, Final Report

Megan Kelley

California Institute of Technology
LIGO Project, MS 18-34
Pasadena, CA 91125
Phone (626) 395-2129
Fax (626) 304-9834
E-mail: info@ligo.caltech.edu

Massachusetts Institute of Technology
LIGO Project, Room NW22-295
Cambridge, MA 02139
Phone (617) 253-4824
Fax (617) 253-7014
E-mail: info@ligo.mit.edu

LIGO Hanford Observatory
Route 10, Mile Marker 2
Richland, WA 99352
Phone (509) 372-8106
Fax (509) 372-8137
E-mail: info@ligo.caltech.edu

LIGO Livingston Observatory
19100 LIGO Lane
Livingston, LA 70754
Phone (225) 686-3100
Fax (225) 686-7189
E-mail: info@ligo.caltech.edu

http://www.ligo.caltech.edu/

1 Motivation

The Laser Interferometer Gravitational-Wave Observatory (LIGO) experiment uses an enhanced Michelson interferometer to determine the relative distance between two test masses that may be perturbed by a passing gravitational wave. At a frequency of 100 Hz, the displacement sensitivity of LIGO's 4 kilometer long arms is $10^{-20}\mathrm{m}/\sqrt{\mathrm{Hz}}$, which is about five orders of magnitude smaller than the classical radius of the proton.[1] The level of precision required to make this measurement effectively requires that all sources of noise be carefully considered and reduced as far as possible. The three primary sources of noise in the experiment are quantum noise (shot noise) dominant at high frequencies, thermal noise dominant at mid-range frequencies, and seismic noise dominant at low frequencies. The seismic noise begins to dominate at about 10 Hz; lower than 10 Hz the noise increases many orders of magnitude, creating what is known as the "seismic wall" on the low end of LIGO's sensitivity band, as seen in Figure 1.

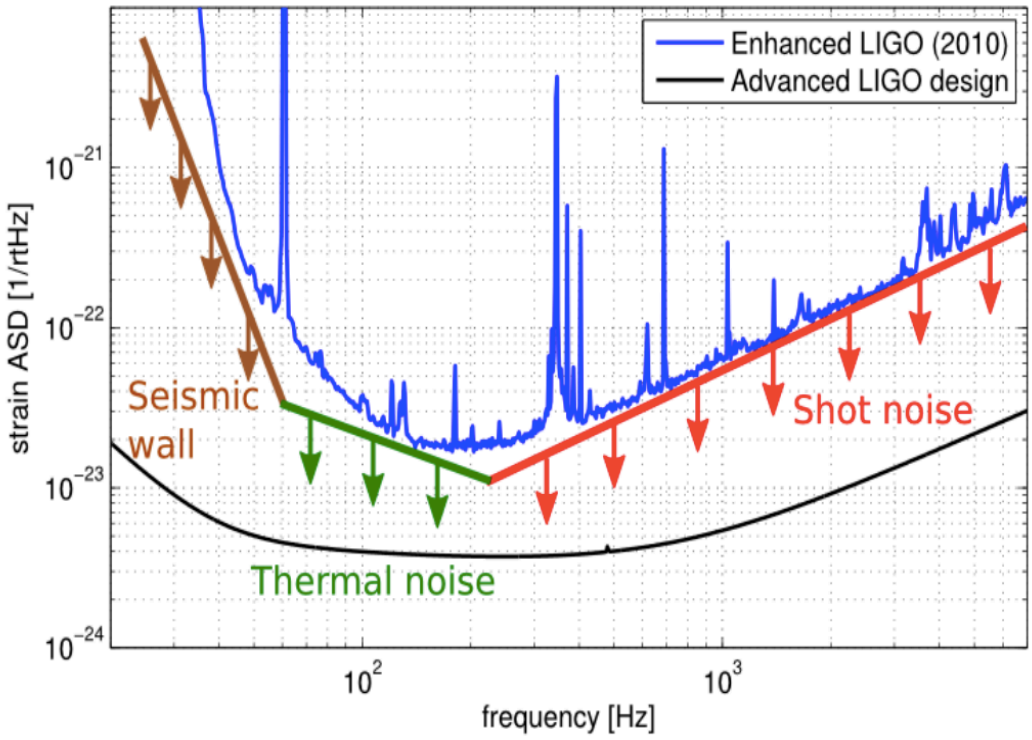

Figure 1: The noise curves for Initial and Advanced LIGO, showing the three main contributors to noise in the three regions.[1]

The sources of this low frequency noise vary from microseisms (ex. ocean waves minutely pushing on the continent), people walking near the detector, and wind on the detector. There is great interest in lowering the seismic noise present in the experiment because continuous

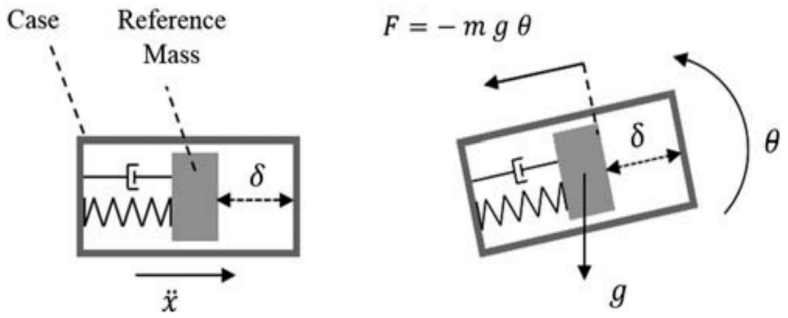

Figure 2: A seismometer subjected to both translation and tilt, and both the translation and the tilt create the same amount of compression in the spring.[2]

sources of gravitational waves, such as closely orbiting neutron stars and black holes, emit waves at low (<10 Hz) frequencies. If LIGO can reduce its seismic noise, a greater range of phenomena will be available for study.

The basic structure of a seismometer is that of a mass that can oscillate about an equilibrium, returned by some restoring force. A simple example of this is a mass on a spring. When the ground moves, the mass is forced into oscillation, and some aspects of the ground's motion can be determined from observing the mass's motion. Two aspects of ground motion that are detected with inertial (mass on a spring) seismometers are ground translation and ground tilt. Especially at low frequencies, the tilt component of ground motion contaminates the desired translation-only reading of the seismometer. In present-generation seismometers, the tilt is subtracted out of the signal via a tilt-sensitive instrument. However, the noise in the this additional instrument often reduces the precision of the data greatly. Therefore, the end goal of this project is to create a 'tilt-free' seismometer that is mechanically insensitive to tilt, in order to remove the necessity for the second, tilt-only measurement.

As described by Matichard et al.,[3] no inertial sensor can fully distinguish between horizontal translation of the ground and tilt of the ground due to the equivalence principle. An observer inside the seismometer would be unable to distinguish seismometer motion caused by tilt from seismometer motion caused by translation, because the vertical component of the local gravitational field would cause motion in the same direction that translation would cause. This tilt-translation coupling can be seen graphically in Figure 2.

However, by clever mechanical design, a sensor that is insensitive to tilt within a certain frequency range can be constructed. The basic design of this sensor is a traditional seismometer in a box that is suspended from a thin wire. The top of the wire is connected to a frame that is rigidly attached to the ground. Assuming a perfect suspension point, the suspended box and seismometer will not move if the ground tilts, but will move if the ground translates. In practice, this method is only effective for ground motion frequencies that are above the resonant frequency of the pendulum formed by the suspended box. So by creating pendula that have very low resonant frequencies, a large range of translational ground motion frequencies can be measured without contaminating tilt motion.

To determine the frequency-space behavior of the pendulum that carries the seismometer,

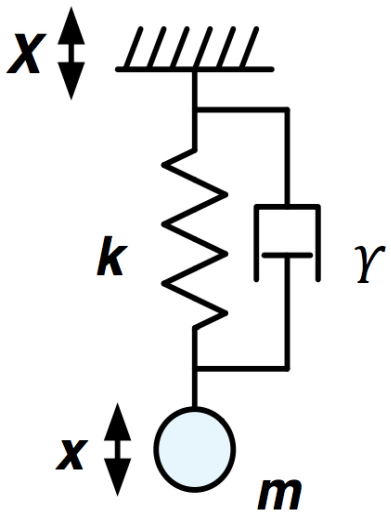

Figure 3: A seismometer consisting of a mass on a spring with some damping mechanism.

its equation of motion must be examined. For this analysis, the pendulum will be treated as a mass on a spring that can oscillate with some damping, as shown in Figure 3. The equation of motion for a damped and driven simple harmonic oscillator is as follows:

$$m\ddot{x} = -k(x - X) - \gamma(\dot{x} - \dot{X}) \tag{1}$$

where x is the motion of the oscillator's mass m with respect to the suspension point, X is the motion of the suspension point (ground motion), $\dot{x}$ and $\dot{X}$ are their time derivatives, $\ddot{x}$ is the second time derivative of x, k is the oscillator's restoring force proportionality constant, and γ is the damping factor. The Fourier transform of this equation of motion is as follows:

$$\frac{\tilde{x}}{\tilde{X}} = \frac{\omega_0^2 + i\frac{\gamma}{m}\omega}{\omega_0^2 + i\frac{\gamma}{m}\omega - \omega^2} \tag{2}$$

where $\tilde{x}$ and $\tilde{X}$ represent x and X in frequency space, ω is the oscillator's frequency, and ω_0 is the oscillator's resonant frequency: $\omega_0 = \sqrt{k/m}$. The plot of this function in frequency space is shown in Figure 4. The general shape of the oscillator's behavior in frequency space is that of a high-pass filter: below the resonant frequency, the response of the oscillator to a given ground motion is large, and above the resonant frequency the response is small. For the frequencies larger than the resonant frequency, the decrease in oscillator response is proportional to g/ω^2. Because the decrease in oscillator response takes effect only above the resonant frequency, it is important to push the tilt resonant frequency as low as mechanically possible. And by creating a pendulum whose resonant frequency is as low as possible, the seismometer at the end of the pendulum will have the greatest range of tilt-free frequencies available for study.

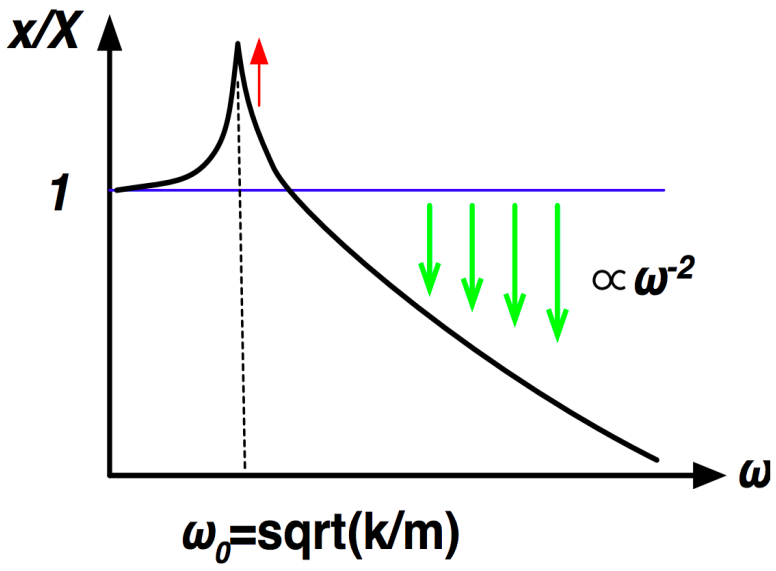

Figure 4: The response of an oscillator (x) to ground motion (X) in frequency space.[4]

2 Summer Project

The project for this summer is to construct a prototype of the theoretical tilt-free seismometer described above. Designs were developed in previous years by Dooley et al.[5]. The design consists of an inverted pendulum on a frame, called the rhomboid, that is suspended from above by thin wires. The relative distance of the pendulum and the rhomboid will be continuously measured via a Michelson intererometer. When the ground translates, the rhomboid is able to swing on its wires, causing the inverted pendulum to move, and register a change of distance in the interferometer. However, when the ground tilts, the orientation of the rhomboid will not change due to its suspension by wires, and no change in distance will be measured by the interferometer. However, due to the fact that no inertial sensor can completely separate tilt and translation, this method is only effective at frequencies above the tilt resonant frequency of the suspended rhomboid.

The interferometer will be a typical Michelson interferometer, in which light travels down two orthogonal arms and is reflected back to the junction of the arms. The resulting interference of the light when it recombines allows the calculation of the relative distance between two objects (in this case the rhomboid and the inverted pendulum). The lengths of the arms of the interferometer must be accurate to less than 1mm, to reduce frequency noise. Fiber coupled light from another optics table goes to the interferometer, where there will be a 10kHz piezoelectric transducer (PZT) actuator. This PZT is used to modulate the length of one of the arms of the interferometer, which produces a known signal to look for at the asymmetric port. This error signal will be fed back to the PZT after being digitized through a control filter and a digital-to-analog converter.

This prototype seismometer will also include an insulative enclosure and a temperature-control system. The operating temperature of the seismometer will be kept at 35°C, roughly

10°C above room temperature. With the seismometer held above room temperature, it will be isolated from environmental effects such as drafts in the room, heat from other instruments in the room, etc. Higher temperatures are typically a significant source of noise, but in this prototype, priority is placed on keeping the temperature constant. In later iterations of the seismometer, more advanced temperature control systems will be implemented in order to reduce thermal noise in addition to holding the temperature constant.

The enclosure will consist of aluminum alloy sheets that cover the frame of the seismometer, two flexible silicone-rubber heaters on opposite inside faces, and foam insulation covering the whole of the frame. A ThorLabs temperature controller will be used to keep the temperature at a desired value.

3 Project Accomplishments

3.1 Thermal Enclosure Construction

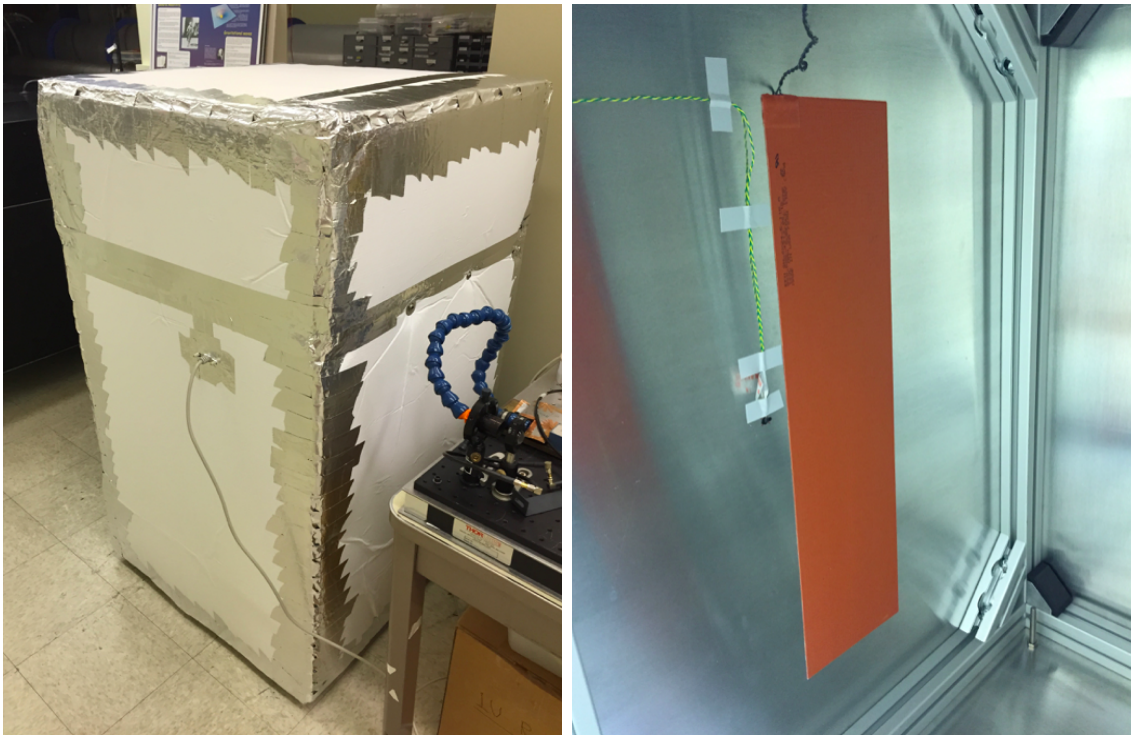

Figure 5: (a) The completed thermal enclosure, sealed with aluminum tape at the corners. (b) The inside of one of the vertical walls of the enclosure. The orange rectangle is one of the heaters, and the small black patch to its left is a thermistor attached with thermal epoxy.

The frame for the seismometer was constructed from 45mm-square aluminum McMaster-Carr extrusion pieces. It is a simple rectangular prism, 36” high and 27.5” wide and deep. There is a crossbar across the top of the frame, for use in suspending the rhomboid. Once the frame was constructed, the method of attaching the aluminum sheets and foam insulation was developed. The sheets, along with the foam on top of them, are attached to the frame

via drop-in spring-held fasteners to the frame, and ∼1” screws. The top portion of the frame, including the cross bar and any supports above it, is enclosed in a lid made of the same aluminum and foam that surrounds the base. The enclosure is supported by four stainless steel feet that are height-adjustable. Figures 5(a) and 5(b) show the finished thermal enclosure, outside and inside.

The temperature control system was implemented by installing four 10kΩ thermistors and two 750W flexible wire-wound heaters inside the thermal enclosure. The heaters were adhered on vertical sides opposite one another, and each had one thermistor adhered near it. Of the remaining two thermistors, one was placed on the lower half of the back wall of the enclosure, and the other was placed on the inside of the front face of the enclosure's lid. The TC200 temperature controller used the signal from one of the thermistors that was near a heater, and a second controller was used solely to measure the signals from the remaining three thermistors. These three signals can be used to compare the temperature in the area of the enclosure that is used in the actual temperature-control loop with the other regions of the enclosure.

3.2 Thermal Calculations

The frame for the seismometer was constructed from 45mm-square aluminum McMaster-Carr extrusion pieces. It is a simple rectangular prism, 36” high and 27.5” wide and deep. There is a crossbar across the top of the frame, for use in suspending the rhomboid. Once the frame was constructed, the attachment of the aluminum sheets and foam insulation were discussed at great length. The sheets, along with the foam on top of them, are attached to the frame via drop-in spring-held fasteners to the frame, and ∼1” screws. The top portion of the frame, including the cross bar and any supports above it, is enclosed in a lid made of the same aluminum and foam that surrounds the base. The last face was left off to allow access to the inside of the seismometer, so that the rhomboid and its associated optics can be installed easily.

A thermal time constant for the enclosure was calculated via basic differential equations. Starting from the simple equation $dQ = mc \cdot dT$ and defining the dQ as the net flow of energy through the system, the following differential equation was calculated:

$$T'(t) = A - BT(t) \tag{3}$$

where the constants A and B are defined as follows:

$$A = \frac{1}{mc}(P_{in} - KA_{side}d_{insul}T_{lab}),\ B = \frac{KA_{side}d_{insul}}{mc} \tag{4}$$

where P_{in} is the power delivered into the system by the heaters, K is the K-factor of the insulation, d_{insul} is the thickness of the insulation, T_{lab} is the constant temperature of the lab room, A_{side} is the area of one face of the frame, m is the mass of the frame and outer layers, and c is the specific heat of aluminum. Solving equation (4) yields the following:

$$T(t) = \frac{A}{B} + C_1 e^{-Bt} \tag{5}$$

which implies that the time constant for the system is the inverse of B. Using estimates for the parameters of the system (seen in Table 1), the time constant was calculated to be 2.25

hours. This is longer than the desired 500 second time constant, so the parameter space of the system must be explored in order to yield a lower time constant. A more complete version of these calculations can be seen in the Appendix.

Variable	Physical Interpretation	Value	Units
K	Thermal conductivity of insulation	58.121	$J/K/s/m^2/m$
A_{side}	Area of one enclosure side	0.75	m^2
d_{insul}	Thickness of insulation	0.0254	m
m	Mass of one side of enclosure's frame	10	kg
c	Specific heat of aluminum	0.9	$J/g/K$

Table 1: Values used in determining the time constant of the thermal enclosure.

3.3 Enclosure Tests

3.3.1 Small-Scale Enclosure Test

The initial tests of the materials used in the construction of the thermal enclosure were done on a small scale. A small (∼6" square by 1" high) hollow box made of aluminum was surrounded by the lightweight melamine insulation that is used in the full-scale enclosure. A small 1" by 5" Kapton resistive heater was adhered to the inside upper face of the aluminum box, and a thermistor was adhered near it. The heater and the thermistor were connected to a ThorLabs TC200 temperature controller.

With only the sides of the aluminum box insulated, the system took about 20 minutes to equilibrate from room temperature to 35°C. With all faces of the box insulated, the equilibration time was about 15 minutes. These initial results show the importance of the insulation in minimizing the system's time constant; with less insulation heat can more quickly leak out of the system. Another aspect of this small-scale test was the investigation of the time constant, and its dependence on both the insulation of the system and the power produced by the heater. More insulation, as well as more power from the heater, decreased the time constant.

3.3.2 Full-Size Heater Test

The heaters used in the full-size enclosure are 6" by 24" flexible silicone-rubber heat sheets from McMaster Carr. To carry out an initial test, the heaters were wired in series and placed under a section of aluminum siding and between sheets of foam. The heaters were then driven with the TC200 temperature controller from room temperature (23.7°C) to a final set temperature (35°C). At the time of writing, there is no way to get temperature-vs.-time data from the TC200 controller, so for the initial heater test data was taken by hand. The data from this test is shown in Figure 6.

The series of black x's in Figure 6 represents the actual temperature of the enclosure, and the blue line represents a theoretical $1 - e^{-t}$ heating curve, with a time constant of 25 minutes. Because the time constant value represents the time it takes for an increasing-temperature

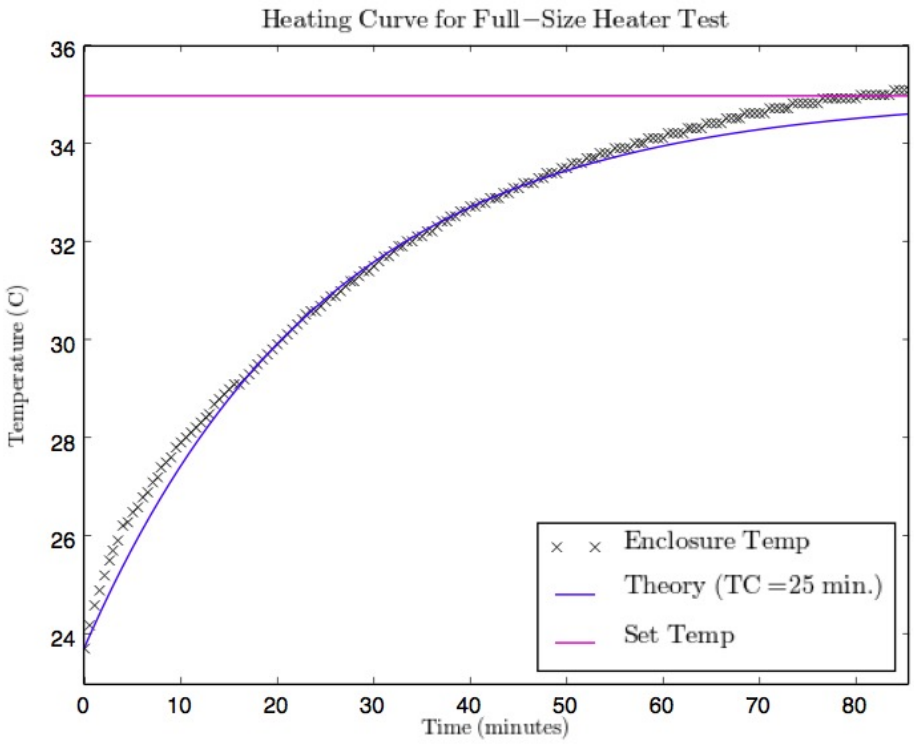

Figure 6: Temperature of the setup as a function of time for the initial test of the full-size heaters.

system to reach $1 - 1/e \approx 63.2\%$ of its final asymptotic value, the time constant of the temperature data can be calculated directly. This value was then used to fit the theoretical curve to the data. After matching relatively closely between 20 minutes and 50 minutes, the theory and the data begin to diverge around the 55 minute mark. This is due to the fact that the data curve eventually reaches the set temperature, while the theory curve only ever asymptotically approaches the set temperature. The differences between these two curves show that the TC200 controller does more than apply power to the heaters until they reach the set temperature; further tests will be needed to determine the controller's process for bringing materials to a given set temperature.

3.3.3 Full-Scale Enclosure Test

Once the enclosure was fully assembled and the heaters and thermistors installed, the first full-scale test of the system was carried out. The data showing the temperature of the enclosure as a function of time is shown in Figure 7. The enclosure began to heat up relatively quickly, but reached a peak of approximately 25°C after about 14 hours. This is a full 10°C short of the target equilibration temperature. Once the enclosure had reached its peak temperature of 25°C, its temperature began to roughly follow the temperature of the room. This lack of stabilization shows that the heated aluminum on the inside of the enclosure has some form of contact with the outside.

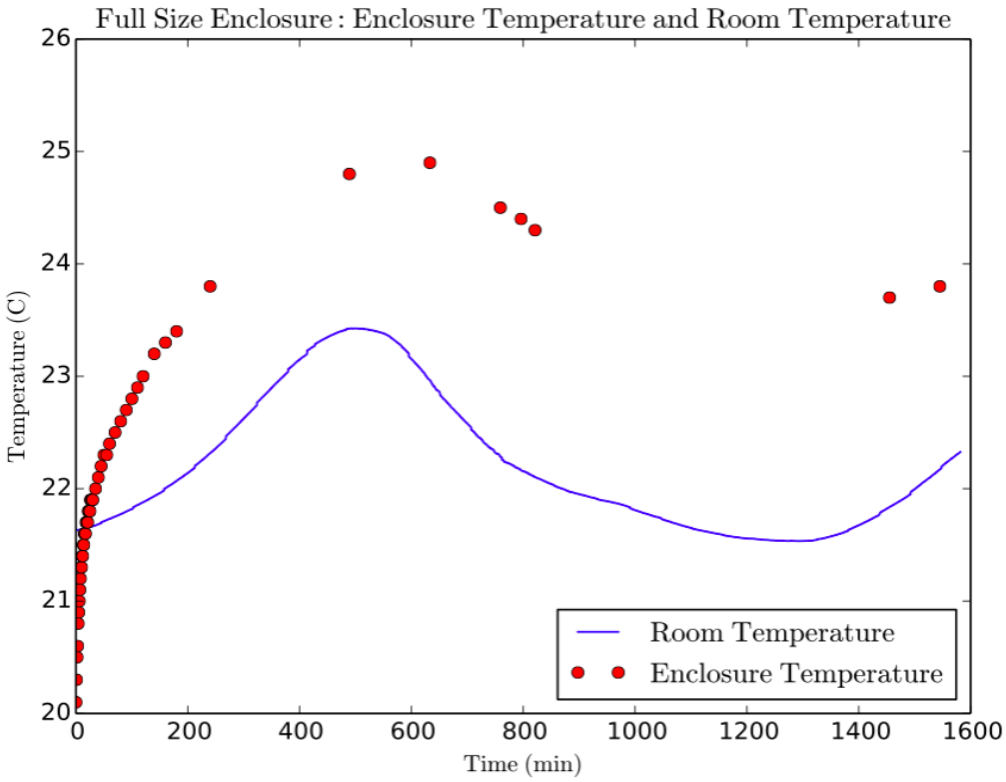

Figure 7: Temperature of the enclosure as a function of time for the first full-scale test.

The thermal conductivity of the foam, or the K from Section 3.2, can be used to quantify enclosure's heat loss. Thermal conductivity is energy transferred per unit time per unit area per unit thickness per degree temperature difference on either side of the insulation. Thus, given the power of the heaters (energy per unit time) and insulation thickness and area, one can calculate the maximum temperature difference that the insulation can support. The calculation goes as follows:

$$\left(\frac{1}{58.121}\frac{\mathrm{K}\cdot\mathrm{s}\cdot\mathrm{m}^2\cdot\mathrm{m}}{\mathrm{J}}\right)\left(18\frac{\mathrm{J}}{\mathrm{s}}\right)\left(\frac{1}{0.75}\frac{1}{\mathrm{m}^2}\right)\left(\frac{1}{0.0254}\frac{1}{\mathrm{m}}\right) = 16.26\,\mathrm{K} \tag{6}$$

where $18\,J/s$ (18W) is the maximum power supplied by the heaters (determined by the maximum power of the TC200 temperature controller), $0.75\,m^2$ is the area of one vertical side of the enclosure, and $0.0254\,m$ is the thickness of the insulation. The theoretical temperature gradient is 16.26°C, but the maximum temperature gradient that was set up in practice was about 5°C. This implies that $16.26/5 \approx 3.25$ times as much heat is being lost than is being contained by the insulation.

To further investigate the lack of the system's stabilization, data was taken as the enclosure cooled down from its maximum temperature. This data is shown in Figure 8. At first glance, it appears to be cooling with a simple exponential decay behavior. However, upon fitting the data points, a double-exponential behavior appears. The fit is as follows:

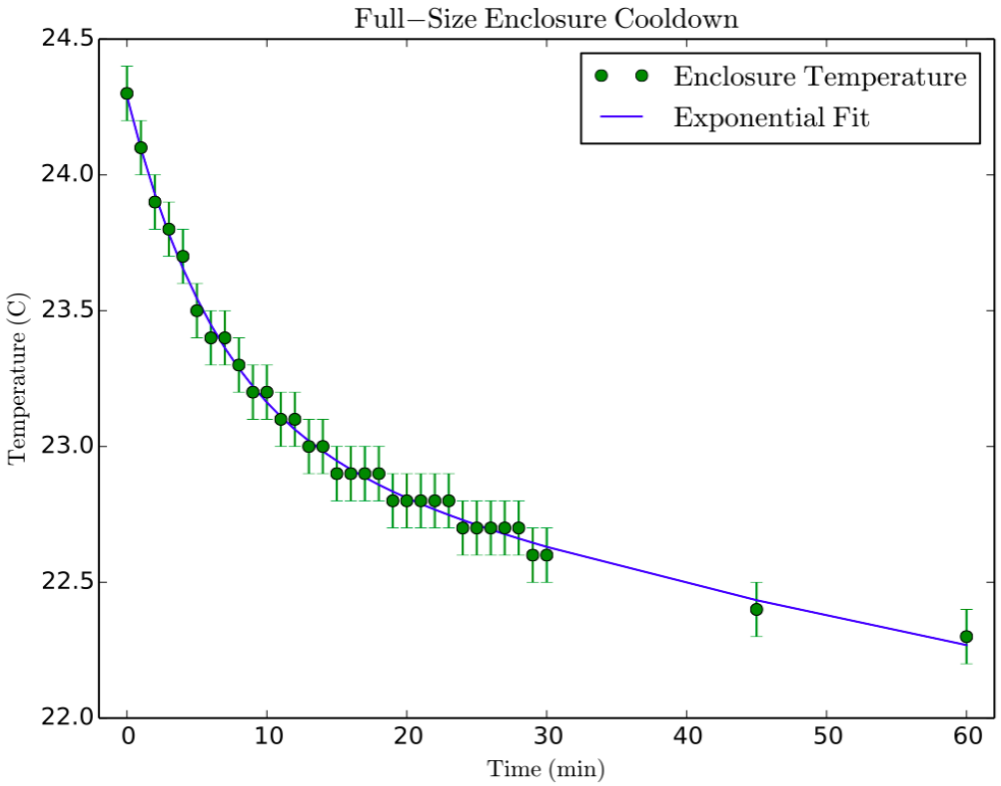

Figure 8: Temperature of the enclosure as a function of time as it cools down from its peak temperature.

$$T(t) = Ae^{-t/B} + Ce^{-t/D} + E \tag{7}$$

where A, B, C, D, and E are positive constants, as shown in Table 2.

Parameter	**Value**	**Function**
A	2.03	First exponential scale factor
B	119.5	First exponential time constant
C	1.22	Second exponential scale factor
D	6.393	Second exponential time constant
E	21.04	$t \to \infty$ equilibration temperature

Table 2: Parameters for the double exponential fit of the enclosure cool down data.

The double exponential behavior demonstrates that the system has two time constants that correspond to two different regimes of cooling. One possible explanation is that heat flows within the enclosure to a region that is in contact with the outside environment, and then the heat flows out into the external environment. This hypothesis is in agreement with the fact that the enclosure has some heat leak, as shown by its inability to reach the set temperature of 35°C.

3.4 Rhomboid Suspension

The rhomboid has been suspended from the outer frame using high-carbon steel wires, secured at the lower end with pin vises and at the upper end with pin vises and plate clamps. A first attempt to suspend the rhomboid resulted in a broken pin vise, but after using epoxy to secure it, the rhomboid was successfully suspended and remained suspended for a long period of time (∼weeks). A new design for wire clamping has been devised; in this new design a collet surrounds the wire, and is tightened around the wire via a small opening in a block of aluminum. The tension from the weight of the rhomboid is counteracted by a peg attached to a worm gear, similar to tuners used on string instruments. This new wire suspension will be implemented on the next iteration of the rhomboid.

Initially, the rhomboid had a very low resonant frequency of about 40 mHz. The tens of millihertz range approaches the lower limit of easily achievable resonant frequencies in mechanical devices, which bodes well for this design. The resonant frequency increased to about 100 mHz as optics were added to the rhomboid, but counterweights were added to diminish the effect. The center of mass of the bare rhomboid is designed to be about 1 mm below the wire connection point, which keeps the system stable. When the optics were added, the center of mass rose above the connection point, which made the pendulum's motion unstable. To combat this, counterweights were added to the bottom-most face of the rhomboid. These weights kept the rhomboid hanging evenly, and also ensured that there would be a restoring force returning the rhomboid to equilibrium.

3.5 Michelson Interferometer

3.5.1 Michelson Design and Assembly

The Michelson interferometer itself will be constructed from two 0° incidence end-mirrors, one 45° incidence beam splitter, and two 45° incidence steering mirrors. Due to the the small size of the rhomboid's top face, the bases for the optics that make up the Michelson needed to be carefully planned and two bases needed to be custom machined for this project. This setup is shown in Figure 9: the laser light enters the system via an optical fiber from the left, and exits the system via the photodetector on the right.

As a comparison to the layout diagram, a photograph of the Michelson built on the breadboard can be seen in Figure 10. It is fairly evident that the small breadboard poses many problems. Even with careful base-position planning, there is little room for any adjustment of the optics that may be necessary when aligning the beam. Also, the thickness of the beamsplitter starts to affect the beam path in such a way that the end mirrors may be required to be in places not allowed by their bases. These problems, along with the problem of weight balance, are what define how the Michelson will be completed.

3.5.2 Fiber Coupling to Michelson

A 500 mW, 1064 nm laser will be used to operate the Michelson. The laser is nominally 500 mW, but due to old age its true power is somewhat less. Additionally, the light travels through several waveplate/beamsplitter junctions, which reduces the beam power to about

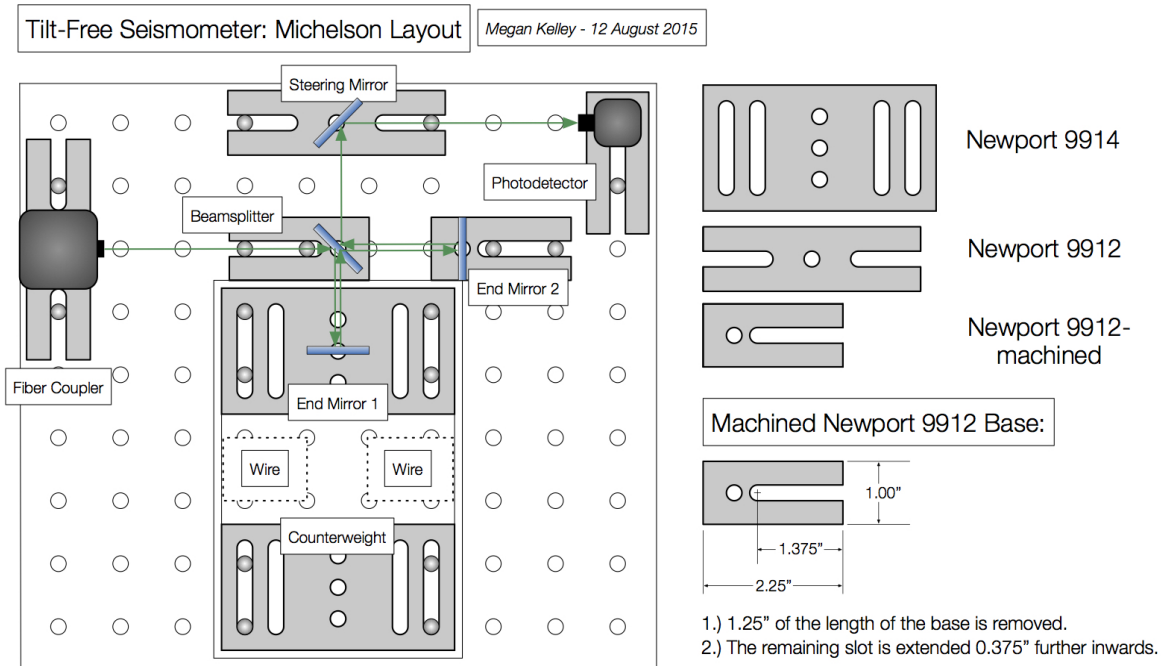

Figure 9: The layout for the Michelson to be placed on the top face of the rhomboid.

75mW once it reaches the fiber. Once the light has been directed to the fiber, the fiber travels between the optics table and the seismometer itself.

In order to get the maximum amount of light from the laser into the fiber, the beam must be mode-matched to the fiber coupler's collimating lens. This can be achieved by taking a beam scan of light coming out of the fiber, then matching the laser with that beam profile. The initial scan of the emerging beam's profile was recorded by moving a CCD along the beam's axis and recording a beam diameter at regular intervals. This data is shown in Figure 11. After the beam shape is well-defined, it can be input to a mode-matching software which will calculate which lenses to use and where to place them in order to match the mode specified.

4 Project Challenges

The biggest challenge of the project has been the design of the thermal enclosure. The basic design, including the layered structure of frame, aluminum sheeting, heaters, and insulation, was well-defined, so the challenges have lain in the specifics of fitting all the layers together. The initial design was to have one sheet of aluminum per face of the frame, but after cutting the aluminum sheeting too short, the design was modified to include a

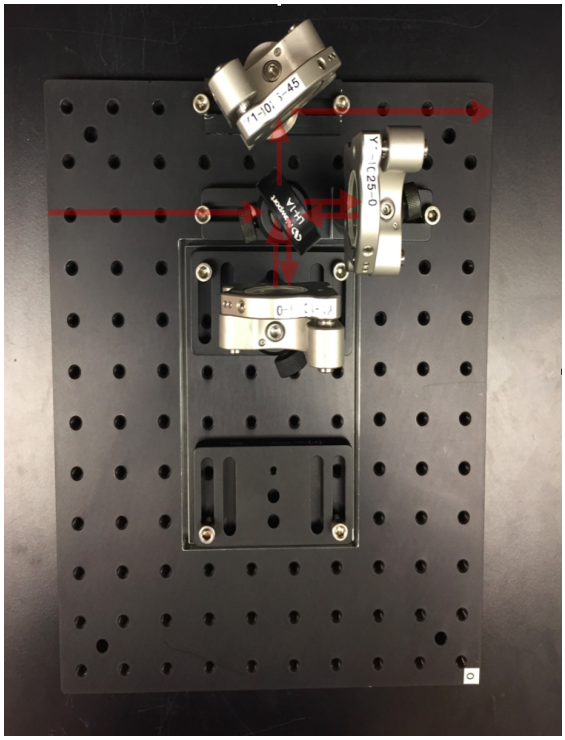

Figure 10: The layout of the actual Michelson on its breadboard.

separate lid component. An added benefit of the lid is accessibility: it offers the ability to access the inside of the seismometer without having to completely remove one of the side panels.

Additionally, the temperature control of the enclosure was challenging given the low power of the heaters and a potential leak in the insulation. A solution to this problem is using a more powerful controller to drive the heaters, and to fix any leaks in the insulation. And if the current insulation is determined to be inadequate, a more suitable foam can be found to replace it.

Another challenge has been the behavior of the suspended rhomboid. When first suspended, it did not hang plumb from the suspension point, rather, it twisted slightly around its two support wires. It also hung slightly higher to one side than the other. The twisting could be due to a wire being attached when it was not fully unwound, and the uneven hang could be due to uneven upper pin vises. Re-suspending the rhomboid after confirming that the wires are not twisted on themselves may fix the twisting problem, while careful weight distribution will fix the uneven hang.

Finally, the placement of the Michelson interferometer on the rhomboid and inverted pendulum poses a challenge because of weight distribution issues, and wiring issues. One of the Michelson's end mirrors will be placed on the upper face of the rhomboid, which brings the center of mass of the rhomboid/inverted pendulum system above the suspension point. This can be counteracted with counterweights on the bottom of the rhomboid, but the major challenge lies in balancing the system in such a way that the resonant frequency of the

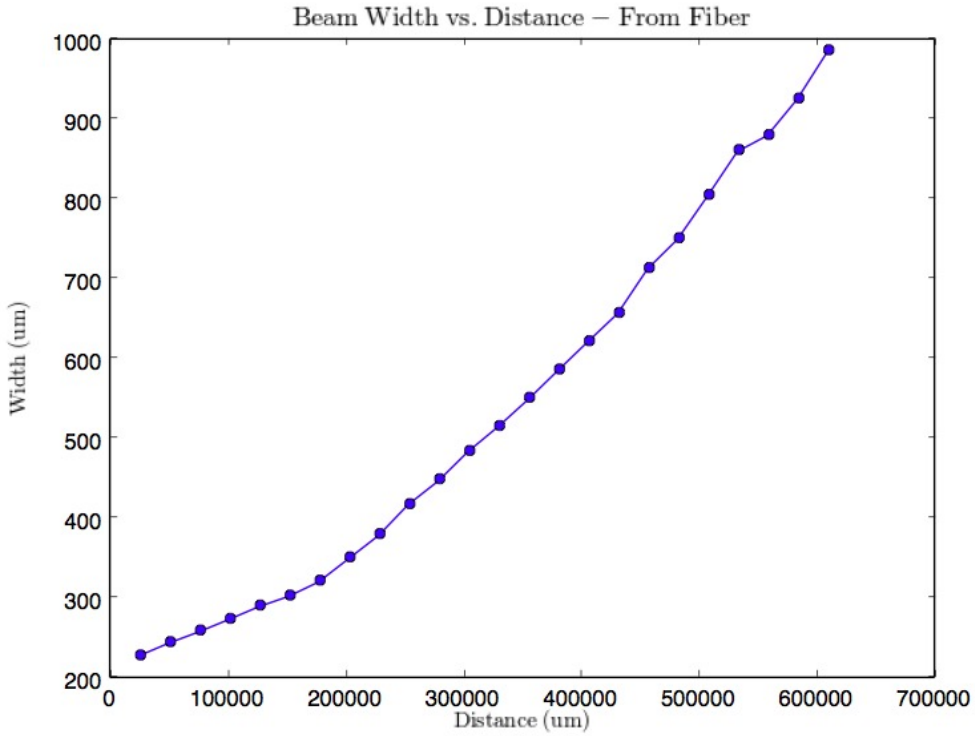

Figure 11: The diameter of the beam emerging from the fiber coupler as a function of distance from the coupler.

system is low (∼40 mHz).

5 Future Work

For the thermal enclosure, future work will involve creating a system that is more capable of temperature control. Obtaining a controller that can drive the heaters to their fullest extent will greatly increase the power input to the system, and creating a more robust insulation system will decrease the enclosure's heat loss to the environment. These two in concert will allow the controller to more precisely control the temperature of the enclosure. But in creating this new system, the accessibility of the interior of the enclosure needs to be kept in mind; the optics inside the enclosure will need to be able to be adjusted easily.

The beam profile scan that was taken on the fiber can be fit with a curve that closely models its shape, and then this curve can be input into the mode-matching software. Once the appropriate lenses and distances have been calculated, the final setup to deliver the laser light into the fiber can be constructed. With this constructed, light can be input into the Michelson interferometer and it can then be calibrated, and eventually assembled inside the thermal enclosure.

6 Appendix

This appendix offers further detail on the calculation of the thermal enclosure's time constant.

Beginning with the relation of heat and difference in temperature:

$$\frac{dQ}{dt} = mc\frac{dT}{dt} \tag{8}$$

This can be rearranged to isolate the temperature of the enclosure as a function of time:

$$T(t) = \frac{1}{mc}\int \frac{dQ}{dt}dt = \frac{1}{mc}\int P \cdot dt \tag{9}$$

where P is the net power flowing in the system, or $P_{in} - P_{out}$. P_{in} is the power supplied by the heaters, and P_{out} is the power lost radiatively through the insulation. P_{in} is a known value, while P_{out} can be calculated via the K-factor, the thickness of the insulation, the area of a side, and the temperature difference between the two sides. Taking all this into account, the differential equation becomes:

$$T(t) = \frac{1}{mc}\Big[P_{in}t - \int_0^t P_{out}dt'\Big] \tag{10}$$

$$T(t) = \frac{1}{mc}\Big[P_{in}t - \int_0^t KA_{side}d_{insul}(T(t') - T_{lab})dt'\Big] \tag{11}$$

Defining the quantities A and B as follows:

$$A = \frac{1}{mc}(P_{in} - KA_{side}d_{insul}T_{lab}),\ B = \frac{KA_{side}d_{insul}}{mc} \tag{12}$$

the differential equation becomes simple to manipulate and solve:

$$T'(t) = A - BT(t) \tag{13}$$

$$T(t) = \frac{A}{B} + Ce^{-Bt} \tag{14}$$

Therefore, the time constant of the system is the reciprocal of B:

$$\frac{1}{B} = \frac{mc}{KA_{side}d_{insul}} \tag{15}$$

References

[1] Abramovici, A.; Althouse, W. E.; Drever, R. W. P.; Gürsel, Y.; Kawamura, S.; Raab, F. J.; Shoemaker, D.; Sievers, L.; Spero, R. E.; Thorne, K. S.; Vogt, R. E.; Weiss, R.; Whitcomb, S. E.; Zucker, M. E., *LIGO: The Laser Interferometer Gravitational-Wave Observatory*. Science, 256, 325-333, 1992.

[2] Matichard, F.; Evans, M. *Review: Tilt-Free Low-Noise Seismometry*. Bulletin of the Seismological Society of America 105.2A (2015): 497-510.

[3] Matichard, F.; Mittleman, R.; Evans, M., *On the mechanical filtering of the transmission of tilt motion from ground to horizontal inertial sensors*. Pre-print for submission to the Bulletin of the Seismological Society of America (2015).

[4] Dooley, K. *Seismic Isolation*. Presentation for LIGO SURF, DCC G1500851-v1, 2015.

[5] Dooley, K.; Moon, S.; Arai, K.; Adhikari, R., *Towards a tilt-free seismometer design*. Poster at March LVC Meeting (2015), DCC G1500315-v1.